



HAL
open science

Multiscale modelling in nuclear ferritic steels: from nano-sized defects to embrittlement

Nicolas Castin, Giovanni Bonny, M. J. Konstantinovic, Alexander Bakaev, Frank Bergner, C. Courilleau, Christophe Domain, Begoña Gomez-Ferrer, J. M. Hyde, Luca Messina, et al.

► To cite this version:

Nicolas Castin, Giovanni Bonny, M. J. Konstantinovic, Alexander Bakaev, Frank Bergner, et al.. Multiscale modelling in nuclear ferritic steels: from nano-sized defects to embrittlement. *Materials Today Physics*, 2022, 27, pp.100802. 10.1016/j.mtphys.2022.100802 . hal-03881996v1

HAL Id: hal-03881996

<https://cea.hal.science/hal-03881996v1>

Submitted on 24 Jan 2023 (v1), last revised 2 Dec 2022 (v2)

HAL is a multi-disciplinary open access archive for the deposit and dissemination of scientific research documents, whether they are published or not. The documents may come from teaching and research institutions in France or abroad, or from public or private research centers.

L'archive ouverte pluridisciplinaire **HAL**, est destinée au dépôt et à la diffusion de documents scientifiques de niveau recherche, publiés ou non, émanant des établissements d'enseignement et de recherche français ou étrangers, des laboratoires publics ou privés.

Multiscale modelling in nuclear ferritic steels: from nano-sized defects to embrittlement.

N. Castin^(1,*), G. Bonny⁽¹⁾, M.J. Konstantinović⁽¹⁾, A. Bakaev⁽¹⁾, F. Bergner⁽²⁾, C. Courilleau^(1,4), C. Domain⁽³⁾, B. Gómez-Ferrer⁽⁴⁾, J.M. Hyde^(5,6), L. Messina⁽⁷⁾, C. Pareige⁽⁴⁾, M.I. Pascuet⁽⁸⁾, B. Radiguet⁽⁴⁾, M. Serrano⁽⁹⁾, L. Malerba⁽⁹⁾

⁽¹⁾ Studiecentrum voor Kernenergie – Centre D'Études de L'énergie Nucléaire (SCK CEN), NMS Unit, Boeretang 200, Mol, B2400, Belgium.

⁽²⁾ Helmholtz-Zentrum Dresden-Rossendorf, Institute of Resource Ecology, Bautzner Landstr. 400, Dresden, 01328, Germany.

⁽³⁾ EDF-R&D, Département Matériaux et Mécanique des Composants (MMC), Les Renardières, Moret sur Loing Cedex, F-77818, France.

⁽⁴⁾ Groupe de Physique des Matériaux, Université et INSA de Rouen, UMR CNRS 6634, B.P. 12, Saint-Etienne Du Rouvray Cedex, 76801, France.

⁽⁵⁾ National Nuclear Laboratory, Culham Science Centre, Abingdon, Oxfordshire, OX14 3DB, UK.

⁽⁶⁾ Department of Materials, University of Oxford, Parks Road, Oxford, OX1 3PH, UK.

⁽⁷⁾ CEA, DES, IRESNE, DEC, Cadarache F-13108 Saint-Paul-Lez-Durance, France.

⁽⁸⁾ Gerencia Materiales - CAC, CNEA/CONICET, Godoy Cruz 2290, C1425FQB, CABA, Argentina.

⁽⁹⁾ Centro de Investigaciones Energéticas, Medioambientales y Tecnológicas (CIEMAT), Avda. Complutense 40, Madrid, 28040, Spain.

Abstract

Lifetime extension of existing nuclear power plants, or new builds, are efficient assets for the fight against climate change. Radiation-induced embrittlement of the steels constituting the reactor vessels, aimed at containing the radioactive fission products, is one of the main limiting factors for safe operation. In support of the fundamental understanding of the phenomena responsible for these degradations, we developed a framework that explains hardening and the subsequent embrittlement by the formation of nano-clusters of minor alloying elements. This is the first in its kind, enabling full predictability of embrittlement for any ferritic material. The core of our theory is a multiscale modelling tool that predicts the kinetics of solute clustering, given the steel chemical composition and its irradiation conditions. We prove that the formation of nano-clusters ensues from atomic transport driven by radiation-induced mechanisms that differ substantially from classical nucleation-and-growth theories. We then shown that the predicted information about solute clustering can be translated into an estimate for radiation-induced embrittlement, via standard hardening laws based on the dispersed barrier model. We demonstrate the validity of our approach by applying it to hundreds of nuclear reactors vessels from all over the world.

1 Introduction

Nuclear power plant lifetime extension and new builds are assets to fight against climate change [1]. The main lifetime limiting factor for nuclear power plants is the integrity of the

steels composing the pressure vessel, as their mechanical properties degrade under neutron irradiation. Reactor pressure vessel (RPV) steels in “western” nuclear power plants, as well as their Russian counterpart, “VVER” steels, become increasingly brittle with increasing irradiation dose at operating temperature [2]. Ferritic steels are also foreseen in new generations of nuclear reactors, where they will be subjected to harsh environments never experienced at large industrial scale before, noticeably in terms of temperature and neutronic dose. Ferritic/martensitic (F/M) steels, candidate materials for fourth generation fission reactors and fusion applications [F, 3, 4], are also subjected to radiation-induced embrittlement. Systematic experimental investigations are not viable, regarding the lack of relevant irradiation facilities and the prohibitive costs associated to large explanatory campaigns. It is hence essential to understand the fundamental processes taking place in ferritic materials under irradiation [B], to ensure a safe extension of the neutron dose, and the design for new applications in harsh conditions.

The most challenging aspect is that all macro- and micro-structure changes start at the nanometer scale [A], or even at the atomic scale [6]. It is indeed well-established that materials degradation under irradiation unfolds from the formation of nano-sized defects (diameter $D = 1-4$ nm) finely dispersed in the bulk (number density $N = 10^{22}-10^{24} \text{ m}^{-3}$), mainly causing hardening and ensuing embrittlement [15]. Such defects result from the diffusion and interaction of radiation-generated point defects between themselves, with the pre-existing microstructure, and with alloying elements and impurities [5, 6]. Atomic transport mechanisms [7, 8] enrich point-defect clusters with Ni, Mn, Si, P and Cu [9]. This is revealed by atom probe tomography (APT) techniques [A, 9-13], illustrated in Fig. 1a, and by small angle neutron scattering (SANS) techniques [14]. These nano-clusters obstruct the motion of dislocations, thereby hindering the blunting of crack tips. The dispersed-barrier hardening model [16] relates the increase $\Delta\sigma_y$ of the yield strength (hardening) with \sqrt{ND} of the nano-clusters. In turn, the shift ΔT in the ductile-to-brittle transition temperature is correlated to $\Delta\sigma_y$ [17]. Thus, if N , D and f are known for a given steel irradiated under known conditions, the corresponding ΔT can be estimated.

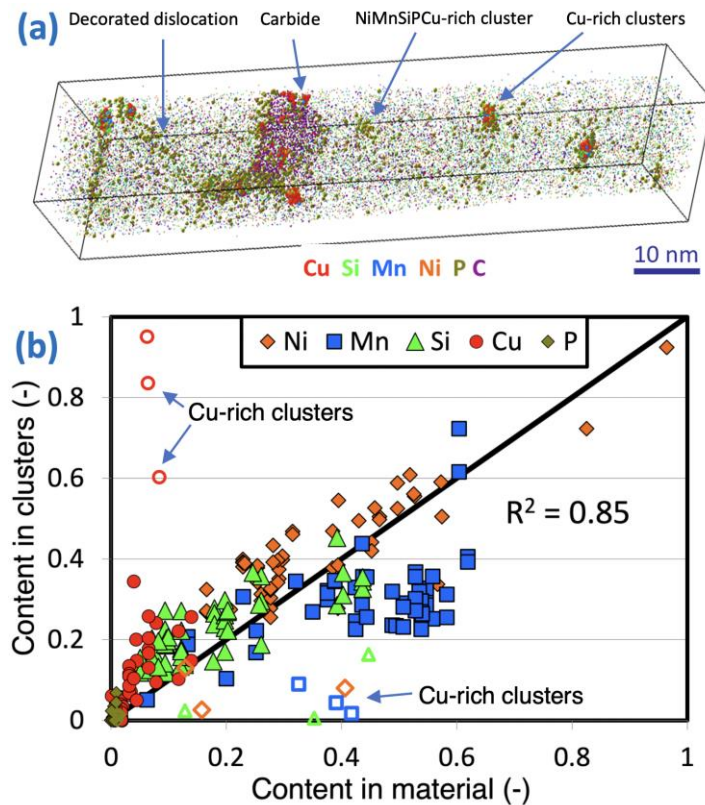


Figure 1 – APT analysis of irradiated RPV steels. (a) 3-D atomic map reconstructed from a Cu-rich irradiated RPV steel. Several radiation-caused features are seen. Typical analyzed volumes contain 2-10 million atoms; (b) correlation between the chemical content in solute clusters in bulk and nominal concentration. Chemical contents are calculated in relative terms, excluding the Fe matrix atoms. Open symbols denote Cu-rich precipitates [18], while closed symbols denote NiMnSiPCu-rich precipitates [9-13].

Thermodynamic-driven precipitation of Cu and Cr occurs under irradiation below 300°C in materials containing more than ~0.1at.% Cu or ~9at.% Cr [4, 19]. In this class of materials, Cu-rich or Cr-rich precipitates are a clear cause of embrittlement [20], and thermodynamic models can be used to predict their formation. We address here the formation of clusters rich in Ni, Mn, Si and P in materials where no element exceeds the solubility limit of the binary alloy. The mechanism of solute cluster formation in this case is still debated. Is it an irradiation-enhanced process, dictated by thermodynamics [21, 22], or an irradiation-induced process that would not occur without irradiation [23, 24]? Recently, Ke *et al.* [22] developed a model based on the assumption that irradiation mainly accelerates the thermodynamics-driven kinetics of phase separation, due to the increased vacancy concentration. This model also included a corrective factor to account for possible “radiation-induced heterogeneous nucleation” of precipitates on point defect clusters produced in atomic displacement cascades. The application of the model revealed that the latter term is dominant by several orders of magnitude over the thermodynamic component, in some cases. This suggests that thermodynamics-driven processes may play a marginal role under irradiation.

APT provides several notable clues for the dominant radiation-induced driving force for solute clustering (Fig. 1):

- a) Segregation is ubiquitous: in addition to finely dispersed clusters in the bulk, high concentrations of solutes (especially P [25]) occur along dislocation segments, at carbides and at grain boundaries.

- b) Two classes of solute clusters can be distinguished by their chemical compositions. The composition of many solute clusters strongly correlates with the overall composition of the material (closed symbols in Fig. 1b). In contrast, in materials with high enough Cu or Cr content, Cu-rich [18, 19] (open symbols in Fig. 1b) or Cr-rich [4] clusters are found.
- c) Clusters are dilute, as they contain a significant fraction of Fe [10, 12, 13]. APT often finds iron contents $\geq 50\%$ [26], while other techniques (electron microscopy, SANS) [14, 26] suggest instead a content $\approx 20\%$ Fe.

These clues advocate for a continuous process of solute deposition on a large density of nucleation sites, triggered and sustained by the continuous fluxes of vacancies and self-interstitials due to irradiation. This mechanism is different from classical precipitation by nucleation and growth and is the foundation of our theory to describe the formation of NiMnSiPCu-rich clusters under irradiation.

The nuclear industry typically employs empirical regressions [35] fitted from experimental data to estimate, given the steel and the irradiation conditions, how ΔT will further evolve with the received neutron dose. Even though they contain some physical information (e.g., explicit terms stand for the so-called “matrix damage”, others for the effects of solute-rich clusters, etc.), their extrapolation capabilities are entirely pending on the choice of the mathematical expressions being used. In this work, we aim at setting the bases for the definition of models more strongly rooted on physics. To this purpose, we develop a multiscale tool for describing the evolution of microstructure under irradiation. We combine first principles calculations, molecular dynamics simulations and atomistic modelling within a single coarse-grained tool that links the atomic to the nanometer scales, allowing for an extension of the simulated time up to decades of neutron irradiation. The tool is therefore driven by elementary, atomic-level reactions, and incorporates all of the above-discussed evidence for radiation-induced clustering. Given the material and the irradiation conditions, it predicts the evolution of N , D and f with the received irradiation dose. From this information, we employ classical hardening laws, also strongly rooted on physics, to correlate this information with the ensuing ΔT . This step can be regarded as a shortcut in the classical multiscale approach [B] towards the desired macroscopic level, substituting the otherwise employed mesoscale methods such as dislocation dynamics, continuous field models or finite elements methods.

2 Material and Methods

2.1 Materials and experimental databases

This work is focused on the following families of materials:

- **Base materials RPV steels:** The pressure vessels of nuclear light water reactors (LWR), i.e. pressurized (P) and boiling (B) water reactors (P/BWR) are made of low carbon ($< 0.9\text{-}1.3$ at%), low-alloyed (> 95 at% Fe) bainitic steels. The main alloying elements common to all RPV steels are Mo (~ 0.3 at%), Ni ($\sim 0.5\text{-}1.0$ at%), Mn ($\sim 0.5\text{-}1.5$ at%), and Si ($\sim 0.2\text{-}0.8$ at%), chiefly added for strengthening purposes. We consider here experimental data from samples irradiated at different dose rates: low and medium, corresponding to surveillance samples ($\sim 2.5 \cdot 10^{-10}$ dpa/s and $\sim 3 \cdot 10^{-9}$ dpa/s), and high, irradiated in an MTR ($\sim 10^{-7}$ dpa/s).

- **Weld materials RPV steels:** these materials are also bainitic steels, but their composition is different, typically they are characterized by higher Ni and Mn content and more impurities; in particular, this class includes steels with very high – for RPV – Ni and Mn content, i.e. up to 2 at%. The irradiation conditions are similar to those of the RPV-BM.
- **Materials used for the RPV of Russian design nuclear reactors (VVER):** these are bainitic steels that contain, in addition to the alloying elements added to western Europe RPV steels, also Cr (~2.0-2.5 at%) and V (0.1-0.35 at%), to provide higher thermal ageing resistance through formation of several types of Cr- and V-containing carbides and carbonitrides. The Ni content varies in a wider range for these materials, as it can be either relatively high (~1.5 at%) or very low (< 0.1 at%). The samples were irradiated in MTR at high dose rate (~ 10^{-7} dpa/s) and in NPP at low dose rates (10^{-10} to 10^{-9} dpa/s).
- **Model alloys for F/M steels,** candidates for future generation IV reactors concepts because of their limited swelling under irradiation and good thermal properties. F-M are characterized by high Cr content (from 2.5at% up to 20at%) and comparatively small concentration of other elements. Typically, among the elements that enter solute clusters, they contain Ni and Si in the 0.1at%-0.2at% range, Mn in concentration ~0.4at%, and P as impurity. Here we considered Fe-Cr-NiSiP model alloys of this family.

Two databases of experimental data were collected from the literature for this work:

- **The microstructure database** collects 94 experimental measurements with APT [Refs] from 44 irradiated materials (30 RPV steels, 10 VVER steels and 4 model alloys for FM steels). For each case, there are 9 input data: the materials chemical composition (Ni, Mn, Si, P and Cu contents in at%), the irradiation conditions (temperature in °C and the dose rate in dpa/s), and the received neutron dose (in dpa, which is equivalent to the irradiation time given the dose rate). The output data are N , D and f of the solute clusters found in bulk, with the associated error bars, measured with APT when available. It is worth noting that SANS measurements are also available for some of the materials studied here. Nevertheless, there are known discrepancies between the measurements of N and D from both techniques, due to their intrinsic functioning and effective resolutions. This effect can be compensated, and it is possible to combine data from both techniques within the same database, but it goes beyond the scope of the present work. See a future publication by C. Courilleau et al. for a detailed analysis.
- **The embrittlement database** collects 1201 experimental measurements from 416 irradiated materials (403 PRV steels, 9 VVER steels and 4 model alloys for FM steels). Most of the data is taken from the PLOTTER database of international nuclear power surveillance [Refs], which is complemented with data found in the literature [Refs]. In the PLOTTER database, we only retained the materials that correspond to a Cu content < 0.1 at%, and for which the received neutron dose reached at least 0.05 dpa. The input data are identical as in the microstructure database, while the output data is the embrittlement ΔT in °C. The specific range of uncertainty associated to each of these measurements should ideally be provided case by case, from the experimental procedures being applied. Since precise information is scarce, we assume that the uncertainty on ΔT is $\pm 25^\circ\text{C}$.

This work aims at predicting the embrittlement ΔT . Experimental data found in the literature often reports the hardening $\Delta\sigma_y$ instead. As both are correlated [17], hardening data is here converted into an estimated embrittlement value with the relation:

$$\Delta T(^{\circ}\text{C}) = 0.5913 \Delta\sigma_y \text{ (MPa)} \quad (1)$$

The coefficient of proportionality was derived from the experimental data in the microstructure database.

2.2 Multiscale model for microstructure evolution under irradiation

In this section, we describe our theoretical model aimed at predicting N , D and f of the solute clusters, as a function of the material chemical composition (Ni, Mn, Si, P and Cu contents in at%), the irradiation conditions (temperature and dose rate), and the received neutron dose (equivalent to the irradiation time, given the dose rate).

The novelty of our approach compared to standard theories (such as, e.g., in [22]) is to explicitly account for the radiation-induced mechanisms discussed above, relying on elementary processes of diffusion, transport and binding at the atomic level. It is implemented through the coarse-grained object kinetic Monte Carlo (OKMC) computational method: see the schematic representation in Fig. 2. The fundamentals of the model were defined in [9], where we demonstrated that the dominant mechanism for nano-cluster formation is the interaction of solute atoms with self-interstitial defects generated under irradiation. Primary point defects (vacancies, self-interstitials and their clusters) are injected in our simulation volume at the right frequency (according to the specified neutron dose rate) using libraries of atomic collision cascade debris previously derived from molecular dynamics. Next, key features are solute transport phenomena induced by the injected point-defects, and their deposition at sinks. When single vacancies or self-interstitials encounter solute atoms dissolved in the matrix, they form stable pairs, with given binding energy. These pairs migrate with given activation energy towards sinks. The characteristic energy values were calculated using density functional theory (DFT) methods [7, 8]. In addition to pre-existing microstructural features, such as dislocations and grain boundaries, point-defect clusters also act as sinks, especially self-interstitial atom clusters (denoted as C1 in Fig. 2). These are immobilized because of strong binding interactions with solute atoms accumulated round them, thereby acting as nuclei for solute clustering.

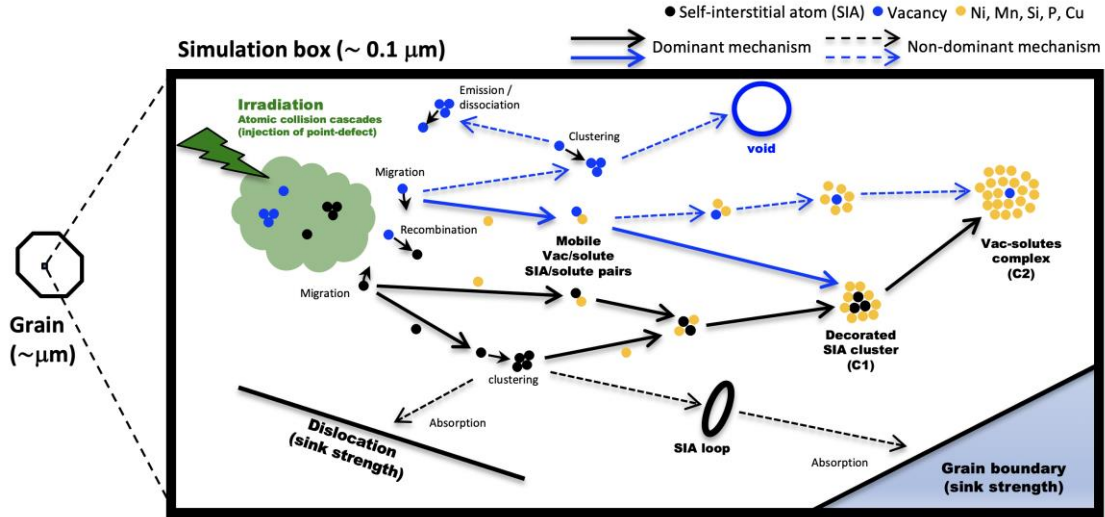


Figure 2 – Schematic description of the object kinetic Monte Carlo method. From left to right, after irradiation events take place, elementary events describe thermally-activated processes of diffusion, dissociation and transport by point-defects, parameterized from first principle calculations. They spontaneously lead to the formation of solute rich clusters: complexes C1 and C2 contain sufficiently atoms to be resolvable with APT. The dominant mechanism [9] of formation is indicated by solid line arrows, while dashed arrows indicate secondary mechanisms which are, formally, not excluded from the model.

While self-interstitial complexes C1 can be safely considered as indissoluble, the dissolution of vacancy-solute complexes C2 (Fig. 2) needs an appropriate description. The corresponding reactions are depicted in Fig. 3. Dissolution is a thermally activated process that takes place via two possible paths: emission of a single vacancy (henceforth denoted as “V”), or emission of a vacancy-solute pair (henceforth “VS”, where S is either Ni, Mn, Si, P or Cu). We estimate the dissociation energy $E_{diss}^{(V,VS)}$ with the well-established approximate relation:

$$E_{diss}^{(V,VS)} = E_m^{(V,VS)} + E_b^{(V,VS)} \quad (4)$$

Here, $E_m^{(V,VS)}$ is the migration energy of a V or VS in bulk Fe, which are known from DFT calculations [7]. In contrast, the binding energy $E_b^{(V,VS)}$ of V or VS to C2 complexes, requires special attention. In the absence of a theoretical framework, the approach in Ref. [9] was to determine them by fitting, taking the binding energies that allows the OKMC model predictions for N , D and f to match the experimental values from APT. The model could therefore only be applied to materials for which detailed microstructure data is known, such as those in the microstructure database described in section 2.1. However, the approach in Ref. [9] cannot be applied to the nuclear power plant surveillance materials collected in the PLOTTER database because, to our knowledge, no APT analysis is available for these materials. As described in section 2.3, in this work we remove this lingering empiricism, and we therefore remove the limits of applicability of our OKMC model. For this purpose, from atomistic modelling and first principle calculations we propose a general recipe to estimate E_b^V and E_b^{VS} a priori, as a function of the chemical composition and the size of the solute clusters.

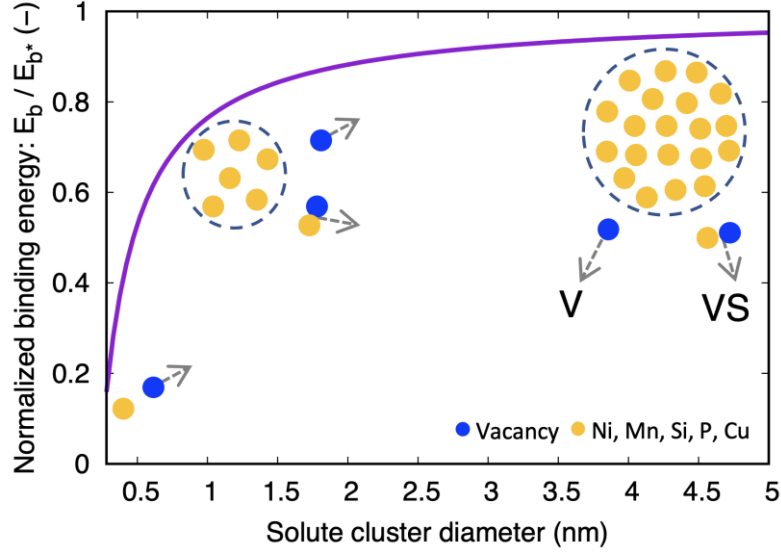


Figure 3 – Schematic description of how the binding energy E_b of vacancies (V) and vacancy-solute pairs (VS) to complexes C2 depend on cluster size. Values are normalized to the saturated value E_{b^*} .

2.3 Determination of key binding energies from atomistic modelling.

The approach to estimate E_b^V and E_b^{VS} as a function of the size of the solute clusters is depicted in Fig. 3. On the left-hand side of the figure, small vacancy-solute complexes are studied using DFT [9]. On the right-hand side of the figure, the other limiting case is a large complex, where the effects of the interface with the Fe matrix do not evolve with size any longer. The corresponding “saturated” binding energy values are denoted as $E_{b^*}^V$ and $E_{b^*}^{VS}$. Intermediate cases can be interpolated using the $V_{C2}^{-1/3}$ capillary law, where V_{C2} is the volume of the complex C2. The OKMC model is therefore fully parameterized once $E_{b^*}^V$ and $E_{b^*}^{VS}$ are known, which solely depend on the chemical composition of the solute clusters.

To calculate $E_{b^*}^V$ and $E_{b^*}^{VS}$, we need a Hamiltonian for an atomic system which contains the Fe, Ni, Mn, Si, Cu and P species. This is offered by the DFT-rooted cluster expansion (CE) model derived in [28]. Given a chemical composition of the C2 complex, we evaluated $E_{b^*}^V$ and $E_{b^*}^{VS}$ using the method developed in [29], which enables the calculation of defect energetics in random alloys on rigid lattice based on an exact mean field approach. This corresponds to assuming that the atoms are randomly distributed inside the complexes, which is a fair assumption, given their mechanism of formation. We applied this method for the materials listed in the microstructure database. Regarding the evidence shown in Fig. 1b, we assume that the relative chemical contents in Ni, Mn, Si, P and Cu are identical to those derived from the overall chemical content of the material. Finally, the Fe content in the solute clusters can be varied between 20 at% and 50at% to cover the limiting cases between experimental evidence from SANS and APT, respectively, without affecting the obtained results. We found that $E_{b^*}^V$ and $E_{b^*}^{VS}$ are strongly correlated with the relative Ni content in the materials, while the content in the other chemical elements play only a secondary role. Looked from that perspective, the values fall within a narrow range of variability. As shown in Fig. 4, it is accordingly possible to write the following estimate functions, which hold for all chemical species (S = Ni, Mn, Si, P or Cu):

$$E_{b^*}^V|_{CE} \cong 1.2 - 0.4 x_{Ni} \pm 0.01 \text{ (eV)} \quad (5)$$

$$E_{b^*}^{VS}|_{CE} \cong 1.56 - 0.85 x_{Ni} \pm 0.15 (1 - x_{Ni}) \text{ (eV)} \quad (6)$$

Here, x_{Ni} is the relative Ni content defined as $C_{Ni} / (C_{Ni} + C_{Mn} + C_{Si} + C_P + C_{Cu})$ and C_{Ni}, \dots, C_{Cu} are the chemical contents in the materials. These estimates could in principle be used directly to parameterize OKMC simulations. However, the superposition of independent migration and binding energies in Eq. (4) does not account for dynamic effects that may affect the true value of $E_{diss}^{(V,VS)}$. To improve accuracy without undue complications, corrections are introduced only on $E_{b^*}^{VS}$. In the OKMC model, we therefore assume that:

$$E_{b^*}^V|_{OKMC} = E_{b^*}^V|_{CE} \quad (7)$$

While an estimate for $E_{b^*}^{VS}$ is derived from another function of the material chemical composition, determined as follows. OKMC simulations were performed for the materials listed in the microstructure database, in the corresponding irradiation conditions. In each case, $E_{b^*}^V$ was taken from Eq. (7) and $E_{b^*}^{VS}$ was varied between $E_{b^*}^V|_{CE}$ and $E_{b^*}^{VS}|_{CE}$ to determine the one that leads to the closest predictions of the solute clusters volume fraction f as compared to the APT data. We demonstrate in section 3.1 that the optimal $E_{b^*}^{VS}$ values can be approximated by another regression of x_{Ni} .

2.4 Determination of embrittlement from solute clustering

According to the dispersed barrier hardening model [16], radiation hardening $\Delta\sigma_y$ can be solely related to the solute clusters that become obstacles for the motion of dislocations. In this work, we apply the model originally proposed by Bacon, Kocks and Scattergood (BKS) [C], as formulated in [D], which considers the elastic interactions between segments of bowed-out dislocations by a population of randomly distributed obstacles. Accounting for Eq (1), we write:

$$\Delta T^{(BKS)} = 0.5913 M \alpha_{BKS}^{3/2} \left(\frac{\ln(\bar{D}/b)}{\ln(l/b)} \right) \frac{\ln(l/b)}{2\pi} \mu b \sqrt{ND} \quad (2)$$

Here, M is Taylor's factor (taken to be 3), l is defined as the free distance between solute clusters ($l = 1/\sqrt{ND} - D$), \bar{D} is a harmonic sum ($\bar{D} = ld / (l + D)$), μ is the shear modulus and b is the dislocation's Burgers vector module. The factor α_{BKS} accounts for obstacles strength by the solute clusters for the flaw of dislocations under the applied strain. Following Friedel's interpretation [D], $\alpha_{BKS}^{3/2}$ can be directly related to the cosine of the bowing angle the dislocations.

The solute clusters diameter D is typically observed to vary within narrow ranges of values in databases of irradiated ferritic steels, at least in the range of temperatures and neutron doses that were studied the most. Considering that $f \approx ND^3/3$ and therefore $\sqrt{ND} \approx \sqrt{f}/D$, for

simplicity and seeking for more accurate regressions, authors [10,11,E] have preferred to rely on this measurement of solute clustering directly. We hence write:

$$\Delta T^{(VF)} = \alpha_{VF} \sqrt{f} \quad (3)$$

Given our embrittlement database described in section 2.1 which provides values for ΔT , and \sqrt{ND} and \sqrt{f} either provided by our microstructure database or estimated by our theoretical model described in section 2.3, numerical values for α_{BKS} and α_{VF} can be estimated from linear regressions.

3 Results

3.1 Final calibration of the multiscale microstructure evolution model

Following the methodology described in section 2.3, we performed OKMC simulations for the materials listed in the microstructure database described in section 2.1. The values for E_{b*}^V are taken from Eq (7) while the values for E_{b*}^{VS} are fitted in such a way that the OKMC predictions of the solute cluster volume fraction f matches the APT measurements. The fitted values are shown by dots in Fig. 4. The error bars indicate the typical range of tolerance for E_{b*}^{VS} to achieve a good match. Interestingly, similarly to the cluster expansion finding in Eq. (5) and Eq. (6), all data collapse around a clearly defined, single average curve, with parabolic shape. These can be estimated with a unique and simple function of x_{Ni} , as follows:

$$E_{b*}^{VS} |_{OKMC} \cong 1.255 - 0.168 x_{Ni} - 0.326 x_{Ni}^2 \pm 0.03 \text{ (eV)} \quad (8)$$

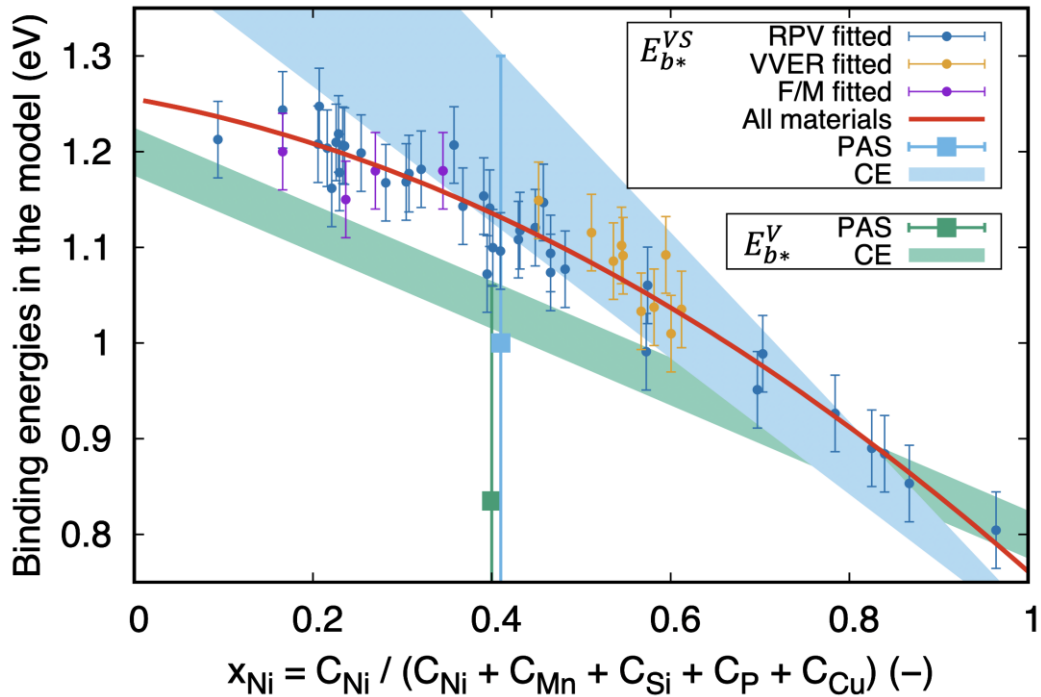


Figure 4 – Saturated binding energy values estimated in different ways, as functions of the relative Ni content in the material. The acronyms PAS stands for positron annihilation spectroscopy (experimental measurement taken from [27]), and CE for cluster expansion (theoretical model based on density functional theory).

Fig. 5 shows a few examples of model predictions of \sqrt{f} versus irradiation dose for different chemical compositions and irradiation conditions. The model matches well the APT data-points and provides estimates for doses that were not investigated experimentally.

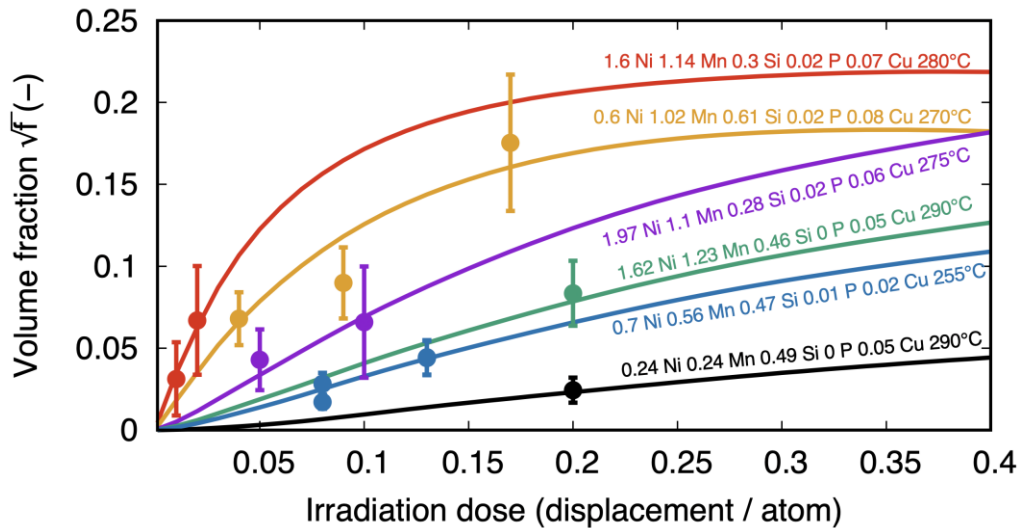


Figure 5 – Application of the microstructure evolution model to the simulation of irradiation experiments in ferritic steels. The individual solid lines (model predictions) depict the evolution with dose of \sqrt{f} related to NiMnSiPCu-rich clusters in bulk, in distinct materials (different colors in the figure). Chemical compositions are given in at%. Dots are experimental measurements with APT taken from the microstructure database.

3.2 Predictions of radiation-induced embrittlement

Via the relations in Eq (2) and Eq (3), the coefficients α_{BKS} and α_{VF} can be determined from linear regressions using a given set of data about solute clusters (N and D), and the corresponding ΔT . We start by performing this exercise using the experimental data from APT collected in the microstructure database. The obtained coefficients are listed in Tab. 1, and the achieved predictions of ΔT are compared with the desired values in the top panels in Fig. 6. Both embrittlement laws appear to correlate the embrittlement ΔT with the amount of solute clustering on the average. Some predictions associated to VVER steels significantly deviate from the desired value, however, but it must be deliberated with the large error bars associated to the APT measurements. Common coefficients are found when RPV and VVER are grouped in the same category of materials, while FM materials should be described by separate coefficients.

Table 1 – Coefficients derived for embrittlement laws using the BKS model or the volume fraction based model. The coefficients are either derived from APT experimental data, or from OKMC estimates, for N and D of the solute clusters. RPV and VVER materials are grouped in a single category, while F/M materials are considered separately. In each case, the 95% interval of confidence (2σ) and the correlation coefficients R_2 are reported.

| | BKS model Eq. (2) | | | Volume fraction model Eq. (3) | | |
|-----------------------|--------------------|----------------|-------|-------------------------------|----------------|-------|
| | α_{BKS} (-) | 2σ (°C) | R_2 | α_{vf} (°C) | 2σ (°C) | R_2 |
| RPV/VVER materials | | | | | | |
| N and D From APT | 0.476 ± 0.088 | 38.6 | 0.838 | 1474 ± 111.1 | 37.2 | 0.840 |
| N and D From OKMC | 0.448 ± 0.024 | 20.7 | 0.922 | 1458 ± 17.94 | 20.8 | 0.920 |
| F/M materials | | | | | | |
| N and D From APT | 0.730 ± 0.409 | 19.6 | 0.806 | 2347 ± 715.7 | 20.3 | 0.886 |
| N and D From OKMC | 0.722 ± 0.126 | 37.4 | 0.942 | 2760 ± 199.3 | 36.6 | 0.945 |

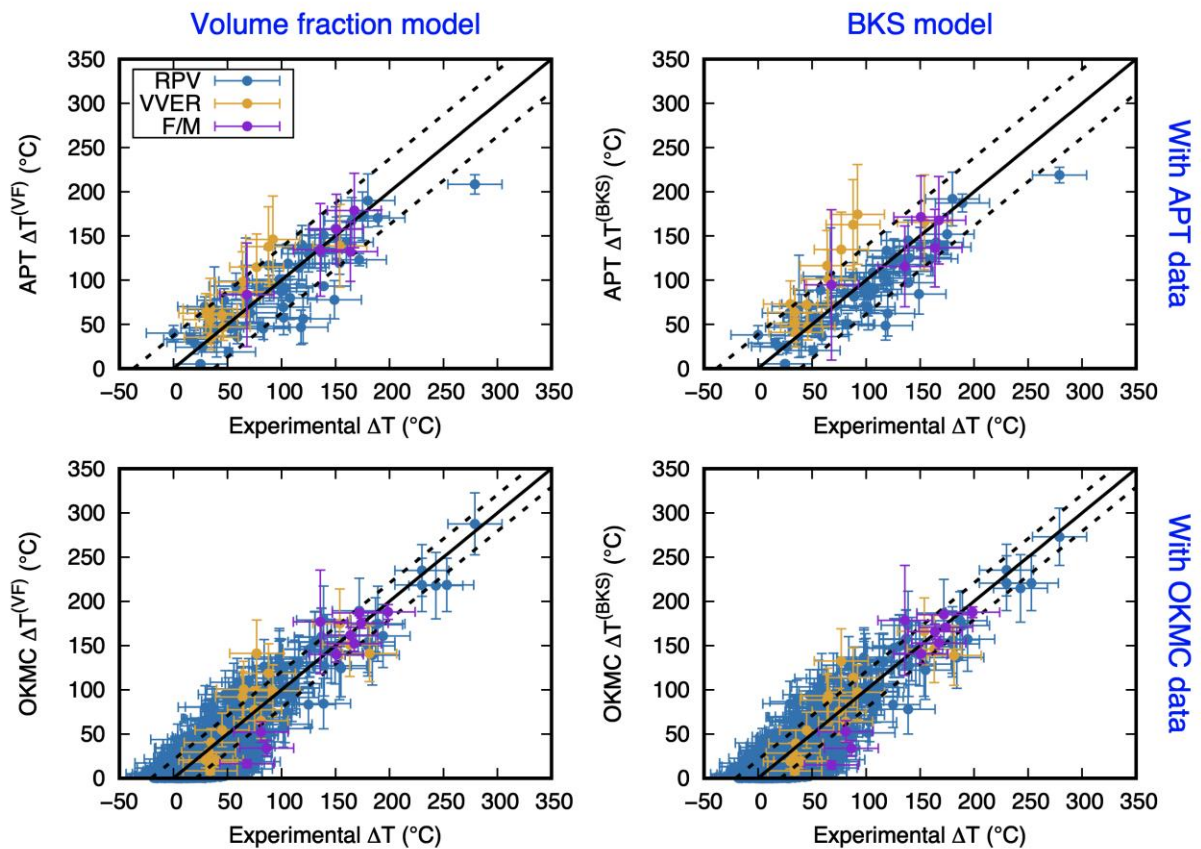


Figure 6— Application of the embrittlement laws from Eq (2) (right panels) and Eq (3) (left panels) using the microstructure database (top panels) and the embrittlement database (bottom panels) described in section 2.1. Black lines are the ideal match, and the dashed lines show the 95% interval of confidence (2σ). The horizontal error bars on the dots is set to 25°C, while the vertical error bars are derived from the experimental uncertainty of the APT measurements or of the OKMC predictions.

Through Eq. (7) and Eq. (8), the OKMC model can be applied without further calibration to the 167 materials and their respective irradiation conditions collected in the embrittlement database. The derived α_{BKS} and α_{VF} are listed in Tab. 1, and the comparison between predicted and target values is shown in the bottom panels in Fig. 6. Remarkably, both embrittlement laws in Eq (2) and Eq (3) work well for nearly all ΔT data-points, with a high accuracy. The discrepancy between predicted and target values is significantly reduced compared to

The coefficients α_{VF} and α_{BKS} are similar to those derived from APT experimental data. It is therefore clear that the linear relations established between \sqrt{f} or $b\sqrt{ND}$ and ΔT are general and can be applied to any material via our theoretical model, without the need of APT data. Importantly, these relations work well also for the high dose data points of the database, suggesting that the model enables accurate extrapolation to higher irradiation doses than those of surveillance. The BKS embrittlement law in Eq. (2), coupled with $b\sqrt{ND}$ computed using the OKMC model, can therefore be used to evaluate the integrity of the pressure vessels in any of the world’s operating nuclear power plants. Examples are shown in Fig. 8, while ??? similar figures are collected in the supplementary information. It is worth noting that the

rightmost irradiation dose of 0.4 displacement per atom correspond to about 80 years of operation for pressurized-water reactors.

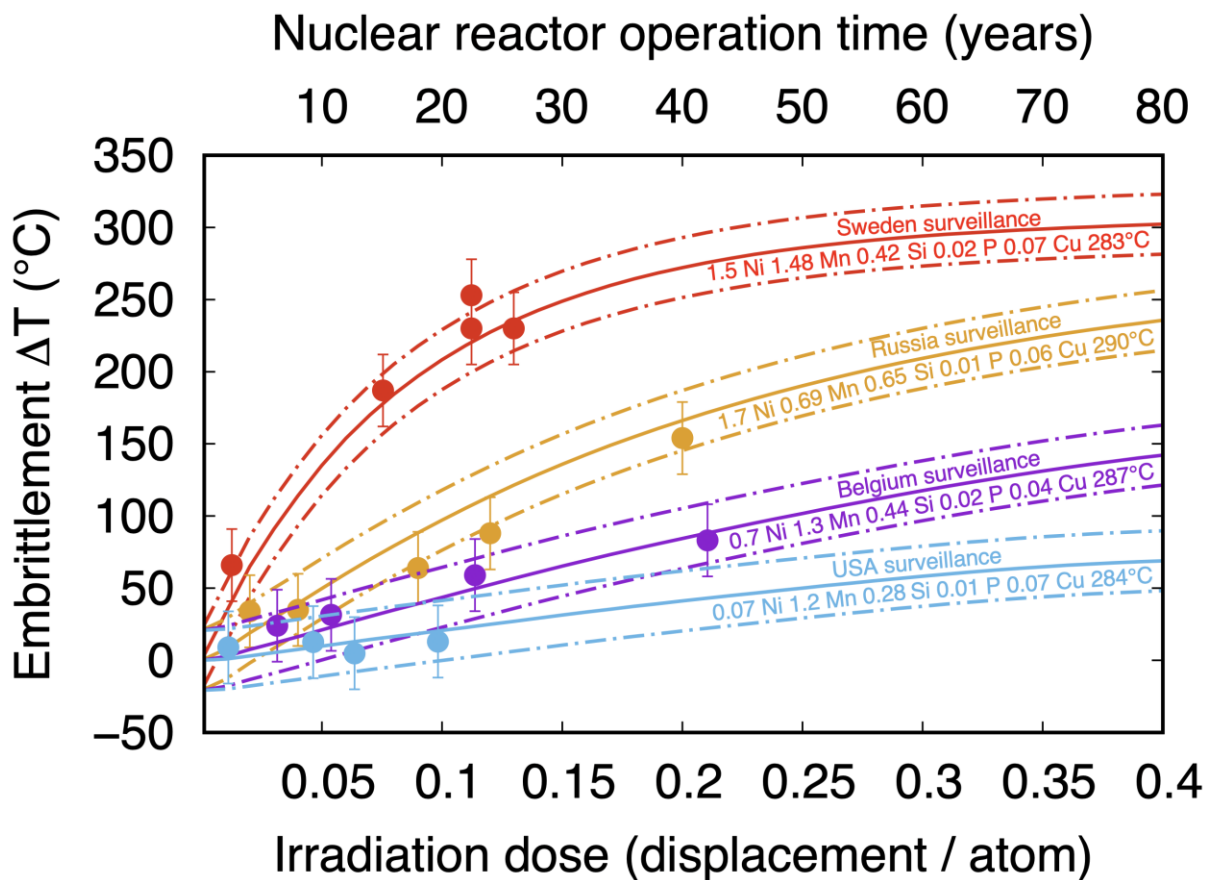


Figure 7 – Physics-based law (BKS model in Eq (2)) for radiation embrittlement applied to individual steels. Evolution with the received dose of the predicted (solid lines) and measured (dots) embrittlement ΔT for four individual steels (different colors). The 95% interval of confidence ($\pm 2\sigma = 20.7^\circ\text{C}$) is shown as well (dashed lines). Chemical compositions are given in at%. The irradiation dose of 0.4 displacement per atoms corresponds to about 80 years of operation for pressurized water reactors. Additional figures for the materials included in Fig. 6 are provided in the [supplementary information](#).

4 Discussion

The theoretical model proposed in this work provides excellent predictions in all cases shown in Fig. 7 and Fig. 8, within an acceptable and constant range of uncertainty. Crucially, the trends versus dose for a given composition are always very well predicted. This strongly suggests that the effect of solute clusters dissolved in the bulk and dragged to sinks is the dominant factor to cause radiation-induced hardening and embrittlement in RPV steels used in nuclear power plants around the world. It is important to discuss the limits of the proposed theory:

- a) The ensuing model is applicable up to 0.1 at%Cu. As discussed above, higher Cu contents imply an increasingly dominant effect of precipitation as dictated by thermodynamics. Consequently, the embrittlement evolution with dose should rapidly saturate and stop increasing, a trend that the model in its present form cannot predict. Instead, the model

would conservatively overestimate embrittlement for these materials, by predicting a continuous growth, as shown in the [supplementary materials](#).

- b) Materials irradiated to doses well beyond those of relevance to RPV steels are known to develop other microstructural features that influence their mechanical properties. For example, near or above 1 displacement per atom, ferritic-martensitic steels develop dislocation loops and nanovoids, which also act as obstacles to the motion of dislocations [33]. While the theory still holds, these additional obstacles are not explicitly accounted for in the present model: embrittlement laws that superpose different defect populations should be applied.
- c) If the P concentration is high enough, its segregation at grain boundaries is known to favor intergranular fracture [34], leading to embrittlement without hardening. This cannot be described by the DBH model adopted here. Such effects should be assessed separately from the effect of bulk precipitation.

The success of our model for different classes of steels has important implications. First, it reveals that the mechanism of solute cluster formation in RPV, VVER, or F/M materials is essentially identical and driven by solute dragging by single point-defects towards sinks. The sinks that dominantly provide nucleation sites for solute clusters are irradiation-generated point-defect clusters. Thus, the radiation-induced character of the process is dominant over the radiation-enhanced one. This conclusion may prove useful for safety assessments in the context of lifetime extension of present nuclear power plants.

Another important implication is that the direct use of microstructural information significantly simplifies the mathematical form of embrittlement-dose correlations: this is evident for instance when comparing [Eq. \(2\)](#) with “classical” correlations used in the industry [35]. The whole dependence of radiation embrittlement on chemical composition, temperature, dose and dose-rate is fully accounted for by \sqrt{f} or $b\sqrt{ND}$, which are computed applying a microstructure evolution theory.

The long-term goal of multiscale approaches [A] is to predict materials behavior with models that describe all fundamental processes along increasing time and space scales. However, the present work suggests that it is also possible to improve the reliability of engineering correlations by directly coupling them with microstructure evolution theories. Specifically, in this work we produced a tool that provides reasonable estimates of microstructural variables, starting from information that is always available (steel composition, temperature, dose and dose-rate), without the need to perform long and costly microstructural examinations (e.g., APT). We argue that, coupled with modern techniques, such as machine learning, it can be directly used for engineering purposes, e.g., providing similar, but faster, predictions of \sqrt{f} or $b\sqrt{ND}$, given the steel and the irradiation conditions [37], or more refined correlations between \sqrt{f} or $b\sqrt{ND}$ and embrittlement, leading to even further reduced uncertainty in the prediction of ΔT .

5 Conclusion

We have developed a robust microstructure evolution theory that quantitatively predicts the formation of solute clusters under irradiation. This piece of microstructural information proves to be sufficient to assess embrittlement as a function of the nuclear power plant operation time. The embrittlement of ferritic steels under irradiation is therefore dominated by the formation of nanometric solute clusters. As such, the embrittlement law provided here in Eq. (2), coupled with our multiscale model for the assessment of solute clustering, can be used to assess the integrity of reactor pressure vessel steels beyond the planned surveillance programs. These predictions will help underpin safety case arguments, enabling the consideration of lifetime extension of existing nuclear power plants, with a positive impact on the fight against climate change [1].

Acknowledgements

This work received partial financial support in the frame of the Euratom research and training programme 2019-2020 including the ENTENTE project (grant No 900018) and H2020-Euratom (grant No 633053); European projects SOTERIA (grant No. 661913), M4F (grant No. 755039), LONGLIFE (grant No. 249360) and MATISSE (grant No. 604862); Joint Programme on Nuclear Materials of the European Energy Research Alliance (EERA JPNM). The views and opinions expressed herein do not necessarily reflect those of the European Commission.

Experiments were performed on the GENESIS platform. GENESIS is supported by the Région Haute-Normandie, the Métropole Rouen Normandie, the CNRS via LABEX EMC and the French National Research Agency as a part of the program “Investissements d’avenir” with the reference ANR-11-EQPX-0020. N. Castin acknowledges Prof. M. Miralles from the Buenos Aires Catholic university (UCA) for a critical review of this work.

Author contributions

N.C., G.B. and L.Ma. led the research. L.Ma. developed the fundamental concepts of the theory. N.C. developed the object kinetic Monte Carlo (OKMC) model. L.Me., C.D. and A.B. derived ab initio data for the development and parametrization of the OKMC model. G.B. and M.I.P. performed atomistic modelling studies that were used to parameterize the OKMC model described in this work. M.K. performed positron annihilation spectroscopy experiments that contributed to the OKMC model parametrization. C.P., B.R. and B.G.F. performed atom probe tomography experiments, F.B. provided small angle neutron scattering data, whose results were used to calibrate the OKMC model. M.K., F.B. and J.M.H. significantly contributed to the development of the embrittlement model proposed in this work. M.S. provided experimental data of radiation embrittlement in steels which were used to validate the embrittlement model proposed in this work. All authors contributed to the writing of the manuscript.

References

- A E.A. Marquis et al., Nuclear reactor materials at the atomic scale, *Materials Today* **12** (2009) 30-37.
- B M. Samaras and M. Victoria, Modelling in nuclear energy environments, *Materials Today* **11** (2008) 54-62.
- C D.J. Bacon, U.F. Kocks, R.O. Scattergood, The effect of dislocation self- interaction on the orowan stress, *Phil. Mag.* **28** (1973) 1241-1263.
- D G. Monnet, Multiscale modeling of irradiation hardening: Application to important nuclear materials, *J. Nucl. Mater.* **508** (2018) 609-627.
- E A. Wagner, A. Ulbricht, F. Bergner, E. Altstadt, Influence of the copper impurity level on the irradiation response of reactor pressure vessel steels investigated by SANS, *Nucl. Instrum. Meth. B* **280** (2012) 98–102.
- F S.J.Zinkle and J. Busby, structural materials for fission & fusion energy, *Materials Today* **12** (2009) 12-18.
- 1 IEA report, Nuclear Power in a Clean Energy System, May 2019, <https://www.iea.org/reports/nuclear-power-in-a-clean-energy-system>
- 2 G.R. Odette, T. Yamamoto, T.J. Williams, R.K. Nanstad, C.A. English, On the history and status of reactor pressure vessel steel ductile to brittle transition temperature shift prediction models. *J. Nucl. Mater.* **526**, 151863 (2019).
- 3 C. Fazio et al. European cross-cutting research on structural materials for Generation IV and transmutation systems. *J. Nucl. Mater.* **392**, 316-323 (2009).
- 4 C. Cabet, F. Dalle, E. Gaganidze, J. Henry, H. Tanigawa, Ferritic-martensitic steels for fission and fusion applications. *J. Nucl. Mater.* **523**, 510-537 (2019).
- 5 C.-C. Fu, J. Dalla Torre, F. Willaime, J.-L. Bocquet, A. Barbu, Multiscale modelling of defect kinetics in irradiated iron. *Nat. Mater.* **4**, 68–74 (2005).
- 6 K. Nordlund et al. Improving atomic displacement and replacement calculations with physically realistic damage models. *Nat. Commun.* **9**, 1084 (2018).
- 7 L. Messina, M. Nastar, N. Sandberg, P. Olsson, Systematic electronic-structure investigation of substitutional impurity diffusion and flux coupling in bcc iron. *Phys. Rev. B* **93**, 184302 (2016).
- 8 L. Messina, T. Schuler, M. Nastar, M.-C. Marinica, P. Olsson, Solute diffusion by self-interstitial defects and radiation-induced segregation in ferritic Fe–X (X=Cr, Cu, Mn, Ni, P, Si) dilute alloys. *Acta Mater.* **191**, 166-185 (2020).
- 9 N. Castin et al. The dominant mechanisms for the formation of solute-rich clusters in low-Cu steels under irradiation, *Mater. Today Energy* **17**, 100472 (2020).
- 10 N. Almirall et al. Precipitation and hardening in irradiated low alloy steels with a wide range of Ni and Mn compositions. *Acta Mater.* **179**, 119–128 (2019).
- 11 N. Soneda, K. Dohi, A. Nomoto, K. Nishida, S. Ishino, Embrittlement Correlation Method for the Japanese Reactor Pressure Vessel Materials. *Effects of Radiation on Nuclear Materials and the Nuclear Fuel Cycle* **24**, 64-93 (PA: ASTM International, West Conshohocken, 2010).
- 12 M.K. Miller et al. Evolution of the nanostructure of VVER-1000 RPV materials under neutron irradiation and post irradiation annealing. *J. Nucl. Mater.* **385**, 615–622 (2009).

- 13 M.K. Miller, K.A. Powers, R.K. Nanstad, P. Efsing, Atom probe tomography characterizations of high nickel, low copper surveillance RPV welds irradiated to high fluences. *J. Nucl. Mater.* **437**, 107–115 (2013).
- 14 S. Mühlbauer et al. Magnetic small-angle neutron scattering. *Rev. Mod. Phys.* **91**, 015004 (2019).
- 15 F. Bergner, C. Pareige, M. Hernández-Mayoral, L. Malerba, C. Heintze, Application of a three-feature dispersed-barrier hardening model to neutron-irradiated Fe–Cr model alloys. *J. Nucl. Mater.* **448**, 96-102 (2014).
- 16 A.K. Seeger, On the theory of radiation damage and radiation hardening. *Proceedings of the Second United Nations International Conference on the Peaceful Uses of Atomic Energy* **6**, 250-273 (1958).
- 17 R.K. Nanstad, W.L. Server, M.A. Sokolov, G.R. Odette, N. Almirall, Some Useful Mechanical Property Correlations for Nuclear Reactor Pressure Vessel Steels. *Proceedings of the ASME 2018 Pressure Vessels and Piping Conference* **6B**, V06BT06A019 (2018).
- 18 M.K. Miller, M.A. Sokolov, R.K. Nanstad, K.F. Russell, APT characterization of high nickel RPV steels. *J. Nucl. Mater.* **351**, 187–196 (2006).
- 19 J.T. Buswell et al. Irradiation-induced microstructural changes, and hardening mechanisms, in model PWR reactor pressure vessel steels. *J. Nucl. Mater.* **225**, 196-214 (1995).
- 20 R.M. Fisher, E.J. Dulis, K.G. Carroll, Identification of the Precipitate Accompanying 885°F Embrittlement in Chromium Steels. *AIME Trans.* **197**, 690-695 (1953).
- 21 P.B. Wells et al. Evolution of Manganese–Nickel–Silicon-Dominated Phases in Highly Irradiated Reactor Pressure Vessel Steels. *Acta Mater.* **80**, 205-219 (2014).
- 22 H. Ke et al. Thermodynamic and kinetic modeling of Mn-Ni-Si precipitates in low-Cu reactor pressure vessel steels. *Acta Mater.* **138**, 10-26 (2017).
- 23 E. Meslin et al. Characterization of neutron-irradiated ferritic model alloys and a RPV steel from combined APT, SANS, TEM and PAS analyses. *J. Nucl. Mater.* **406**, 73-83 (2010).
- 24 H.F. Huang, B. Radiguet, P. Todeschini, G. Chas, P. Pareige, Atom Probe Tomography characterization of the microstructural evolution of a low copper reactor pressure vessel steel under neutron irradiation. *MRS Online Proceedings Library* **1264**, 518 (2010).
- 25 E.A. Marquis, J.M. Hyde, Atomic Scale Analysis of Solute Behaviours by Atom-Probe Tomography. *Mater. Sci. Eng. R Rep.* **69**, 37-62 (2010).
- 26 P.D. Edmondson, C.M. Parish, R.K. Nanstad, Using complimentary microscopy methods to examine Ni-Mn-Si precipitates in highly-irradiated reactor pressure vessel steels. *Acta Mater.* **134**, 31-39 (2017).
- 27 M.J. Konstantinović et al. Radiation induced solute clustering in high-Ni reactor pressure vessel steel. *Acta Mater.* **179**, 183-189 (2019).
- 28 G. Bonny, C. Domain, N. Castin, P. Olsson, L. Malerba, The impact of alloying elements on the precipitation stability and kinetics in iron based alloys: An atomistic study. *Comput. Mater. Sci.* **161**, 309–320 (2019).
- 29 G. Bonny, N. Castin, M.I. Pascuet, Y. Çelik, Exact mean field concept to compute defect energetics in random alloys on rigid lattices. *Physica B Condens. Matter* **517**, 25-29 (2017).

- 30 PLOTTER database, Adjunct for E900-15 Technical Basis for the Equation Used to Predict Radiation-Induced Transition Temperature Shift in Reactor Vessel Materials, <https://www.astm.org/BOOKSTORE/ADJUNCT/ADJE090015-EA.htm>
- 31 R. Chaouadi, R. Gérard, E. Stergar, W. Van Renterghem, Neutron irradiation hardening of chemically-tailored RPV steels with respect to Cu/P and Ni/Mn elements. *J. Nucl. Mater.* **519**, 188-204 (2019).
- 32 V. Kuksenko, C. Pareige, P. Pareige, Cr precipitation in neutron irradiated industrial purity fe-cr model alloys. *J. Nucl. Mater.* **432**, 160–165 (2013).
- 33 E. Gaganidze, J. Aktaa, Assessment of neutron irradiation effects on RAFM steels. *Fusion Eng. Des.* **88**, 118–128 (2013).
- 34 Z. Lu, R. Faulkner, R. Jones, P. Flewitt, Radiation- and Thermally-Induced Phosphorus Inter-Granular Segregation in Pressure Vessel Steels. *J. ASTM Int.* **2**, 1-15 (2005).
- 35 N. Soneda, 11 - Embrittlement correlation methods to identify trends in embrittlement in reactor pressure vessels (RPVs), Irradiation Embrittlement of Reactor Pressure Vessels (RPVs) in Nuclear Power Plants. *Woodhead Publishing Series in Energy* **2015**, 333-377 (2014).
- 36 Y. Li, S. Hu, X. Sun, M. Stan, A review: applications of the phase field method in predicting microstructure and property evolution of irradiated nuclear materials. *Npj Comput. Mater* **3**, 16 (2017).
- 37 N. Castin et al. Advanced atomistic models for radiation damage in Fe-based alloys: Contributions and future perspectives from artificial neural networks. *Comput. Mater. Sci.* **148**, 116–130 (2018).